Highly exposed {001} facets of titanium dioxide modified with reduced graphene oxide for dopamine sensing

Gregory Thien Soon How[1], Alagarsamy Pandikumar[1], Huang Nay Ming[1] & Lim Hong Ngee[2,3]

[1]Low Dimensional Materials Research Centre, Department of Physics, Faculty of Science, University of Malaya, 50603 Kuala Lumpur, Malaysia, [2]Department of Chemistry, Faculty of Science, Universiti Putra Malaysia, 43400 UPM Serdang, Selangor, Malaysia, [3]Functional Device Laboratory, Institute of Advanced Technology, Universiti Putra Malaysia, 43400 UPM Serdang, Selangor, Malaysia.

Titanium dioxide (TiO_2) with highly exposed {001} facets was synthesized through a facile solvo-thermal method and its surface was decorated by using reduced graphene oxide (rGO) sheets. The morphology and chemical composition of the prepared rGO/TiO_2 {001} nanocomposite were examined by using suitable characterization techniques. The rGO/TiO_2 {001} nanocomposite was used to modify glassy carbon electrode (GCE), which showed higher electrocatalytic activity towards the oxidation of dopamine (DA) and ascorbic acid (AA), when compared to unmodified GCE. The differential pulse voltammetric studies revealed good sensitivity and selectivity nature of the rGO/TiO_2 {001} nanocomposite modified GCE for the detection of DA in the presence of AA. The modified GCE exhibited a low electrochemical detection limit of 6 μM over the linear range of 2–60 μM. Overall, this work provides a simple platform for the development of GCE modified with rGO/TiO_2 {001} nanocomposite with highly exposed {001} facets for potential electrochemical sensing applications.

Dopamine (DA) is an important catechol-amine neurotransmitter (NT) in the mammalian central nervous system that influences the central nervous function, attention span, cognition, emotions and neuronal plasticity[1]. Since a network of NTs involves transmission of messages between neurons, disturbance in the dopaminergic system causes neurological disorders in the human body. Recent studies suggests that DA deficiency in the mammalian system leads to the Parkinson's disease, schizophrenia, drug addiction and HIV infection[2,3]. Electrochemical methods are more often used in clinical tests to find out the concentration of DA because of its high electrochemical activity. However, problem arises due to DA as it is usually present in lower concentrations amounts along with high amounts of ascorbic acid (AA) in biological tissues[4]. The conventional electrodes are inefficient for the detection of DA since they give a low response signal due to sluggish electron-transfer rate and also provide overlapping voltammetric response for both DA and AA because of their similar oxidation potential[5]. Therefore, exploring a modified electrode with high sensitivity and good selectivity is the most essential for efficient electrochemical detection of DA in the presence of AA.

Titanium dioxide (TiO_2) is an attractive electrode material and hence it is widely used in a number of electrochemical applications. Due to its good biocompatibility and catalytic properties, TiO_2 has been predominantly employed as an electrode material in electrochemical biosensors for the detection of various analytes even at their lower concentration. Meanwhile, graphene has been equally regarded as an attractive material and its hybridization with TiO_2 as a nanocomposite for DA sensing has gained immense interest, as it offers improved electron transfer and excellent electrocatalytic activity towards the oxidation of DA and distinguishability between DA and interference materials[6,7]. However, these reports focused on the anatase phase of TiO_2 which is usually dominated with thermodynamically stable {101} facets. It is understood that anatase TiO_2 have different facet orientations in a truncated tetragonal bipyramid structure consisting of six {101} facets and two {001} facets and the surface energy estimated for the {101} facets is significantly lower than that of the {001} facets (0.44 J m^{-2} for {101} and 0.96 J m^{-2} for {001})[8]. Recent research works have explored that increasing the exposed {001} facets of TiO_2 leads to better performance in applications such as lithium ion storage and photocatalysis owing to the improved activity of TiO_2[9,10]. To the best of our knowledge, there is no report exist on the study of graphene-TiO_2 nanocomposite with highly exposed {001} facets for DA sensing application. In view of the above facts, in this work, we introduce a simple synthetic route to prepare a reduced graphene oxide (rGO) decorated TiO_2

nanocomposite with highly exposed {001} facets. The rGO/TiO$_2$ nanocomposite was used to modify glassy carbon electrode (GCE) and its electrochemical performance was studied towards the detection of DA in the presence of AA. The results of the study suggest that the GCE modified by using rGO/TiO$_2$ nanocomposite with highly exposed {001} facets could be employed as a potential electrode material for electrochemical sensing applications.

Results & Discussion

Morphological studies of rGO/TiO$_2$ {001} nanocomposite. The morphological features of the prepared TiO$_2$ {001} and rGO/TiO$_2$ {001} nanocomposite materials were studied based on the FESEM images (see Supplementary Fig. S1 online). It is observed from the FESEM images that TiO$_2$ nanostructures with spherical morphology were formed through our synthesis method and the individual spherical TiO$_2$ nanostructures were joined together to form clusters of TiO$_2$. In the case of rGO/TiO$_2$ {001} nanocomposite, the surface of rGO was completely covered by the TiO$_2$ nanostructures (Fig. S1c). However, the inconsistency of the TiO$_2$ structures was clearly seen in Fig.S1d as it exhibits the presence of both TiO$_2$ nanoparticles and folded TiO$_2$ nanosheets in the form of white wire-like structures. To elucidate the presence of {001} facets in TiO$_2$ and its high resolution morphology, HRTEM images were recorded. The HRTEM image of the pristine TiO$_2$ nanostructure (Figure 1a and 1b) is in good agreement with its corresponding FESEM image. It is obviously clear from the HRTEM image of TiO$_2$ that the inner sphere was packed with TiO$_2$ nanoparticles whereas the TiO$_2$ nanosheets were located on the surface of the clustered TiO$_2$. The formation of such structure occurs due to the Oswald ripening process and also the use of DETA as the

morphology controlling agent. The DETA plays an important role by prohibiting the growth of TiO$_2$ along the (001) planes and thereby extending its surface area as the sides increase in length[11,12]. Figure 1c shows an edge of the TiO$_2$ nanosheets, revealing a visible lattice fringe width of 0.19 nm that can be attributed to either (002) or (200) planes of TiO$_2$. With similar method followed by Chen et al.[9], the TiO$_2$ spheres formed were with almost 100% of their exposed {001} planes. For the rGO/TiO$_2$ {001} nanocomposite, similar results were obtained in Figure 1d and 1e. At high resolution in Figure 1f, lattice fringe of 0.19 nm was observed, which can be attributed to the {001} facets of the TiO$_2$ nanosheets[13,14].

Raman studies of rGO/TiO$_2$ {001} nanocomposite. The Raman spectra of GO, rGO and rGO/TiO$_2$ {001} nanocomposite are shown in Figure 2. The Raman spectrum of GO shows well referred documented D band peak at 1353 cm^{-1}, due to the sp^3 defects and an another peak of G band at 1597 cm^{-1}, which can be ascribed to the inplane vibrations of sp^2 carbon atoms and a doubly-degenerated phonon mode (E$_{2g}$ symmetry) at the Brillouin zone centre[15]. It was also demonstrated that the D band peak remains unchanged while the G band peak of rGO was downshifted from 1597 cm^{-1} to 1587 cm^{-1}, owing to the "self-healing" characteristics of the rGO that recovers the hexagonal network of carbon atoms with defects[16]. This confirms the successful reduction of GO to rGO. The second order of zone boundary phonons or 2D band which is related to the stacking nature of graphene layers was observed at 2706 cm^{-1} for GO. The peak was broadened for the rGO/TiO$_2$ {001} nanocomposite as a consequence of multilayer rGO sheets stacking caused by the decrease in the functional groups attached to the rGO, which prevents the sheets from restacking together[17]. In addition, the
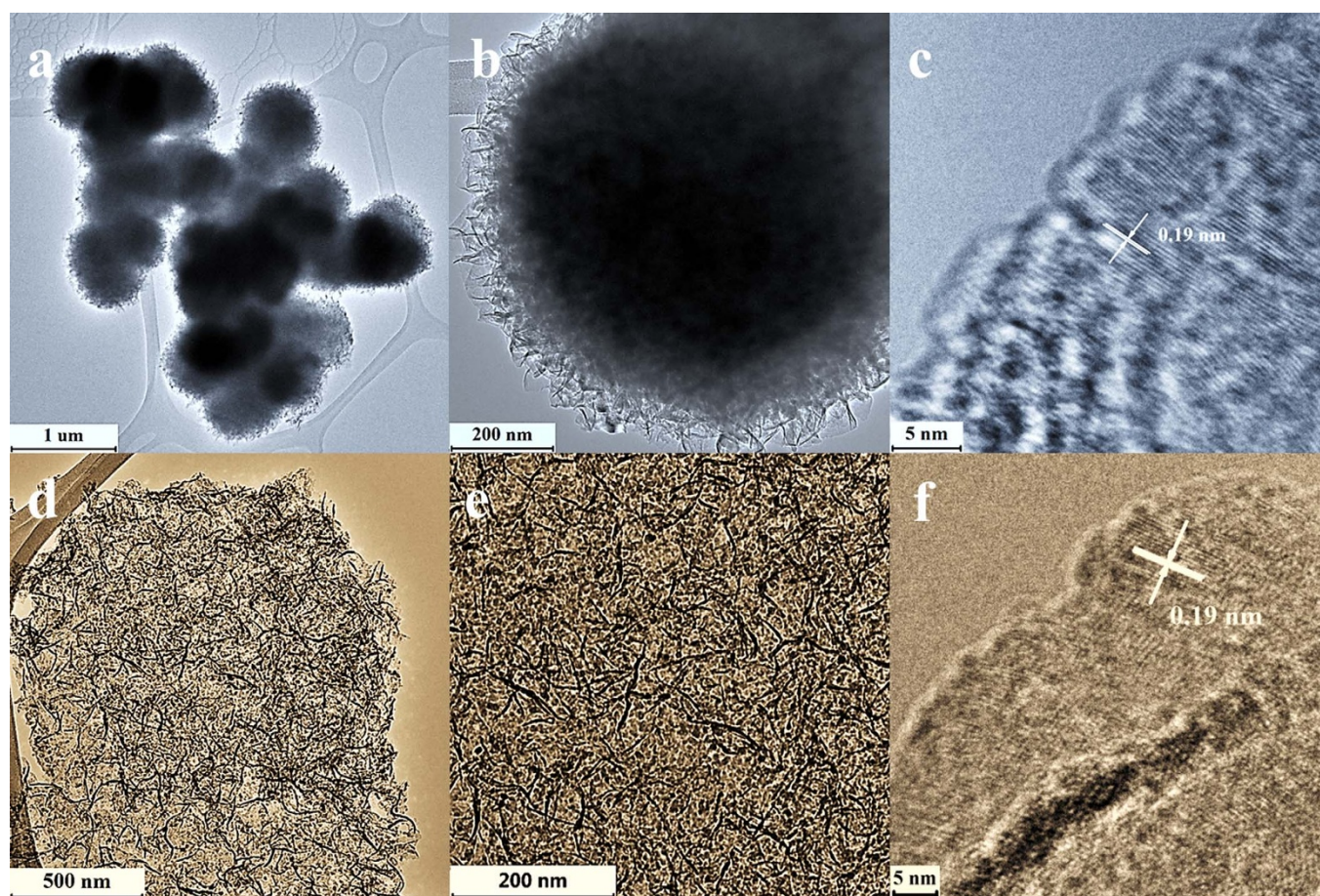

Figure 1 | (a, b) Low magnification TEM images of TiO$_2$ and (c) high magnification TEM image of the edge of a TiO$_2$ nanosheet. (d, e) Low magnification TEM image of the rGO/TiO$_2$ {001} nanocomposite and (f) high magnification TEM image of the surface of the nanocomposite.
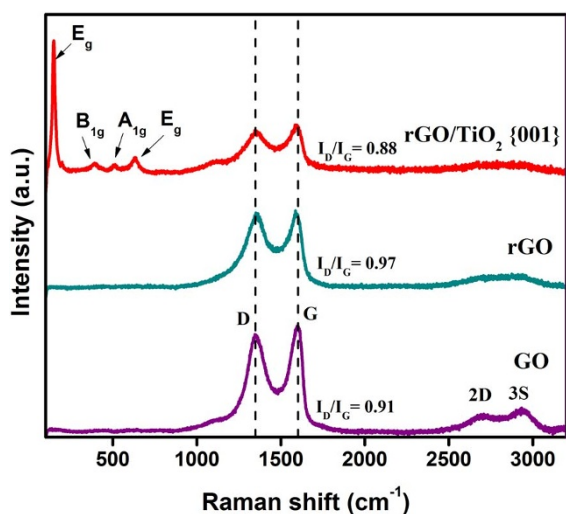
Figure 2 | Raman spectra of GO, rGO, and rGO/TiO₂ {001} nanocomposite.

I_D/I_G ratio was used to measure structural disorder which was slightly increased from 0.91 to 0.97 during the reduction of GO to rGO. As a result, the formation of defects occurs in addition to the removal of oxide functional groups attached to the GO surface[18]. However, a slight decrease in the I_D/I_G ratio was observed as 0.88 for the rGO/TiO₂ {001} nanocomposite because of the decrease in the sp² domain size of carbon atoms and the reduction of sp³ to sp² carbon during the solvo-thermal process[19,20]. Moreover, the presence of E_g, B_{1g}, A_{1g} and E_g modes in the rGO/TiO₂ {001} nanocomposite implies the existence of anatase phase TiO₂[22].

XPS analysis of rGO/TiO₂ {001} nanocomposite. The chemical analysis of the prepared nanomaterials was carried out by XPS (Figure 3). Figure 3a and b shows the core level spectra of C 1 s for GO and rGO/TiO₂ {001} nanocomposite and their peak positions were observed at binding energies of 284.5, 286.2, 287.8 and 289 eV corresponding to the C–C, C–O, C = O and O = C–O bonds, respectively[21,22]. However, the difference in the peak intensities of the oxide functional groups was noticed as they decreased substantially for the rGO/TiO₂ {001} nanocomposite, indicating the successful reduction of GO to rGO during solvo-thermal process. Moreover, a peak emerges at 282.4 eV (Ti-C) which could be contributed by the chemical bonding between titanium and carbon. The chemical states of Ti(IV) species was investigated further and are shown in Figure 3c and d. The Ti 2p core levels can be deconvoluted to a doublet (Ti 2p₃/₂ and Ti 2p₁/₂) and that records a binding energy difference (ΔE_{BE}) of 5.7 eV, which indicates the presence of normal states of Ti(IV) and is consistent with the earlier report[23]. However, the ΔE_{BE} was displaced to the right for the rGO/TiO₂ {001} nanocomposite and the binding energy increases due to the interaction between Ti and the oxide functional groups of rGO, since the oxygen has a higher electronegativity when compared to carbon[24].

Formation mechanism of rGO/TiO₂ {001} nanocomposite. To understand the formation mechanism of the rGO/TiO₂ {001} nanocomposite, a schematic representation was depicted in Supplementary Fig. S2 online. In this synthetic route, GO, TIPT and DETA were chosen as starting materials. However, it was found out that the order of using these materials greatly influenced the resultant desired morphology of the nanocomposite. It was remarkably interesting as when GO undergoes either route A or B, either an inhomogeneous or homogeneous dispersion of rGO/TiO₂ {001} was obtained. The difference was signified at the timing of the

DETA addition into the dispersed GO solution. As DETA is known as a reducing agent, the addition of DETA before the formation of TiO₂ on rGO (route A) reduces active sites of GO to rGO by recovery of hexagonal network of the C atoms. Hence, when the Ti(IV) precursor solution was added, only a partial of the Ti atoms react with rGO to form TiO₂, leaving behind residues of pure TiO₂ and rGO in the composite. Using a modified synthesis in route B, it allows complete formation of TiO₂ nanostructures attached on rGO sheets, which then prohibits facet growth along the {001} direction by addition of DETA, resulting in a homogenous dispersion of the rGO/TiO₂ {001} nanocomposite.

Electrochemical characteristics of the rGO/TiO₂ {001} modified GCE. The electrochemical property of the modified GCEs was investigated in the presence of 0.1 M KCl and 1 mM K₃[Fe(CN)₆] (see Supplementary Fig. S3 online). It was observed that the redox current response towards the ferricyanide ion was higher for the rGO/TiO₂ {001} nanocomposite modified GCE when compared to the bare GCE. This indicates that the rGO/TiO₂ {001} nanocomposite on the GCE surface was positively charged and therefore significantly improved the ferricyanide ions adsorption on the GCE surface[25]. In addition, the peak potential separation, ΔE_p, was estimated for bare GCE, rGO, rGO/TiO₂ {101}, and rGO/TiO₂ {001} modified GCE to be 468, 84, 80, 72 mV, respectively. This reveals that the rGO/TiO₂ {001} modified GCE has the fastest electron kinetic transport. The introduction of rGO/TiO₂ {001} on the GC electrode surface facilitates the enhanced conduction pathway at the modified electrode. On the other hand, rGO/TiO₂ {001} on the GCE surface can act as superior electron transfer medium and thereby enhance the electron transfer efficiently.

Electrochemical impedance spectroscopic (EIS) measurements were performed to investigate the electrochemical behaviors of the different modified electrodes. Fig. S4a shows Nyquist plots obtained for the various modified electrodes. Among these, the bare GCE, TiO₂ {101}, and TiO₂ {001} showed large semicircles, which were due to the large charge-transfer resistance (R_{ct}) at the electrode/electrolyte interface due to the sluggish electron transfer kinetics. This charge-transfer resistance has a negative impact on the electrocatalytic performance[26]. It can obviously be seen that R_{ct} decreased for the rGO, rGO/TiO₂ {101}, and rGO/TiO₂ {001} modified electrodes, which can be attributed to the presence of highly conductive rGO sheets on the GCE surface. Fig. S4b shows the Bode-phase plots of the various modified electrodes in the frequency range of 0.1–10000 Hz. A higher phase peak intensity can be seen at a frequency range of 100–1000 Hz, which can be attributed to the charge-transfer resistances of the pristine semiconductor (TiO₂ {101} and TiO₂ {001}). The large semicircles of the Nyquist plots (Fig. S4a) for the TiO₂ {101} and TiO₂ {001} modified electrodes, corresponding to the high-frequency phase peaks at 100–1000 Hz in the Bode plots, suggest that the charge transfer resistance takes place at the electrode/electrolyte interface. Interestingly, the phase peaks in the Bode plots for the rGO, rGO/TiO₂ {101}, and (f) rGO/TiO₂ {001} modified electrodes shifted to a low-frequency region of 0.1–100 Hz because of the high electron transfer behavior of the rGO-based modified electrodes[27].

Electrochemical oxidation of DA at the rGO/TiO₂ {001} modified GCE. Cyclic voltammograms were obtained for the bare GCE, TiO₂ {101}, TiO₂ {001}, rGO, rGO/TiO₂ {101}, and rGO/TiO₂ {001} modified GCEs in the presence of 0.5 mM DA, and the observed results are shown in Figure 4. The bare GCE showed a quasi-reversible and poorly defined redox peaks because of the sluggish electrochemical response toward DA. However, a significant increase (∼5-fold) in the redox peak current was noted for the rGO/TiO₂ {001} modified GCE, owing to the improved electron transfer process[28]. Meanwhile, a ∼2-fold increase in the redox peak current
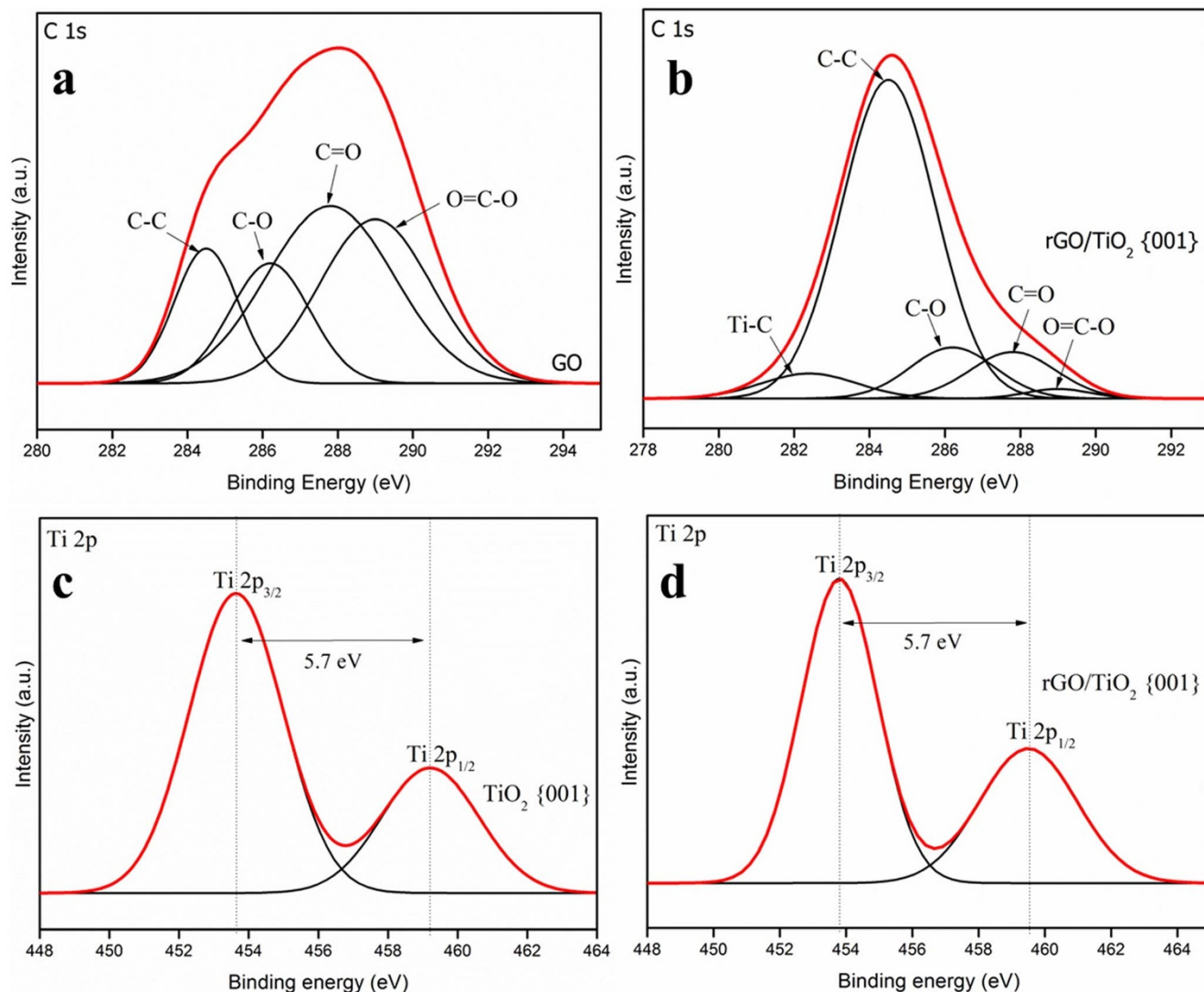
3

Figure 3 | XPS spectra obtained for (a and b) C 1 s core level of GO and rGO/TiO$_2$ {001} nanocomposite, respectively. (c and d) Ti 2p core level of TiO$_2$ {001} and rGO/TiO$_2$ {001} nanocomposite, respectively.

was observed for the rGO/TiO$_2$ {001} modified GCE over the GCE modified by using rGO and rGO/TiO$_2$ {101}, which suggests that the rGO/TiO$_2$ {001} nanocomposite with the highly exposed {001} facets of TiO$_2$ induced better electrical conductivity between the electrode and electrolyte interface. The values for the peak potential separation, ΔE_p, were calculated as 320, 235, 230, 80, 65, and 60 mV for the bare GCE, TiO$_2$ {101}, TiO$_2$ {001}, rGO, rGO/TiO$_2$ {101}, and rGO/TiO$_2$ {001} nanocomposite modified GCE, respectively. Hence, the rGO/TiO$_2$ {001} modified GCE exhibited a reversible behavior and possessed faster electron transfer kinetics as a consequence of its low ΔE_p value[6]. Moreover, the low oxidation peak potential exhibited by the rGO/TiO2 {001} modified GCE (0.19 V) when compared to the bare GCE (0.32 V) and rGO modified GCE (0.20 V) implies that the rGO/TiO$_2$ {001} modified GCE has a better electrocatalytic oxidation behavior towards DA[29].

A schematic representation of the electrocatalytic oxidation of DA at the rGO/TiO$_2$ {001} modified GCE is shown in Figure 5. Dopamine (DA) is easily oxidized electrocalytically and forms dopamine quinone (DAQ) at the rGO/TiO$_2$ {001} modified GCE. When a potential is applied to the electrode, DA is easily oxidized to form DAQ after the exchange of 2 electrons and 2 protons. Later, these electrons are donated to the electrode and produce a faradaic current[30]. The rGO/TiO$_2$ {001} modified GCE
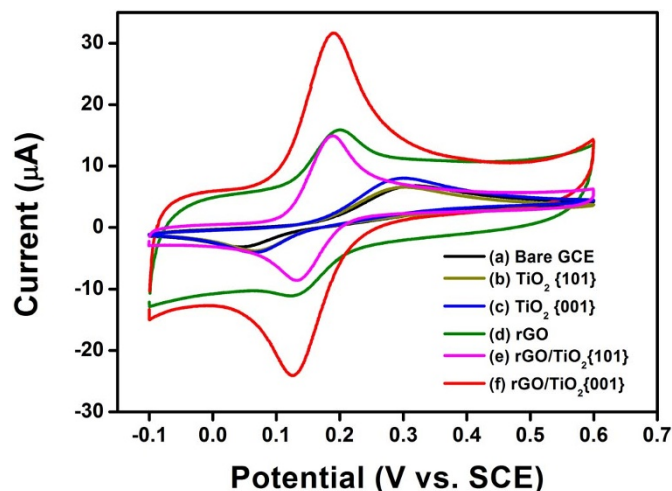

Figure 4 | CVs of (a) bare GCE, (b) TiO$_2$ {101}, (c) TiO$_2$ {001}, (d) rGO, (e) rGO/TiO$_2$ {101} and (f) rGO/TiO$_2$ {001}modified GCE using 0.5 mM DA in 0.1 M PBS (pH = 6.5) at scan rate of 100 mV/s.
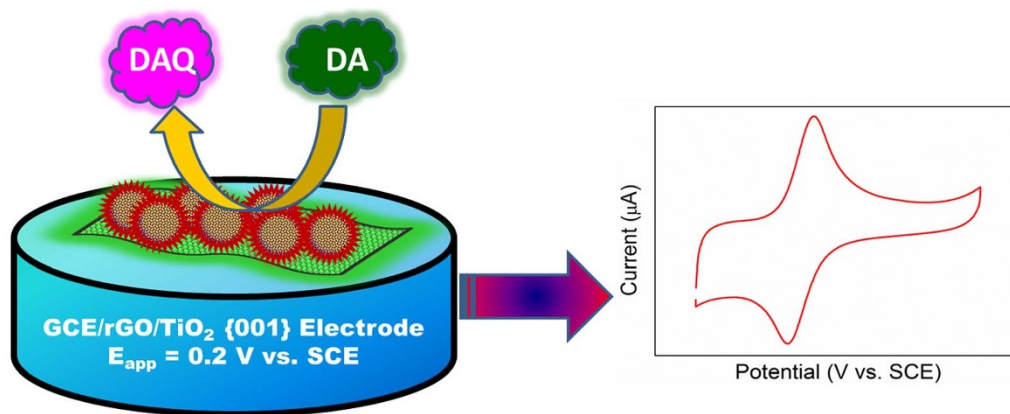
Figure 5 | Mechanism for electrocatalytic oxidation of dopamine at rGO/TiO$_2$ {001} modified GCE.

had better electrocatalytic activity toward dopamine oxidation compared to the other electrodes. The combination of TiO$_2$ {001} and rGO enhanced the electronic conductivity and DA accessibility, which promoted the electron transfer rate between the DA and electrode surface, and thereby caused a good synergistic effect in the electrocatalysis.

Influence of scan rate towards DA oxidation. Figure 6a shows the CV response towards electrocatalytic oxidation of DA in the presence of rGO/TiO$_2$ {001} modified GCE at different scan rates between 10 and 1000 mV s^{-1}. As the scan rate increases, the oxidation and reduction peak currents increase linearly. The linear relationship (R^2 = 0.996 and 0.998) between the redox peak currents
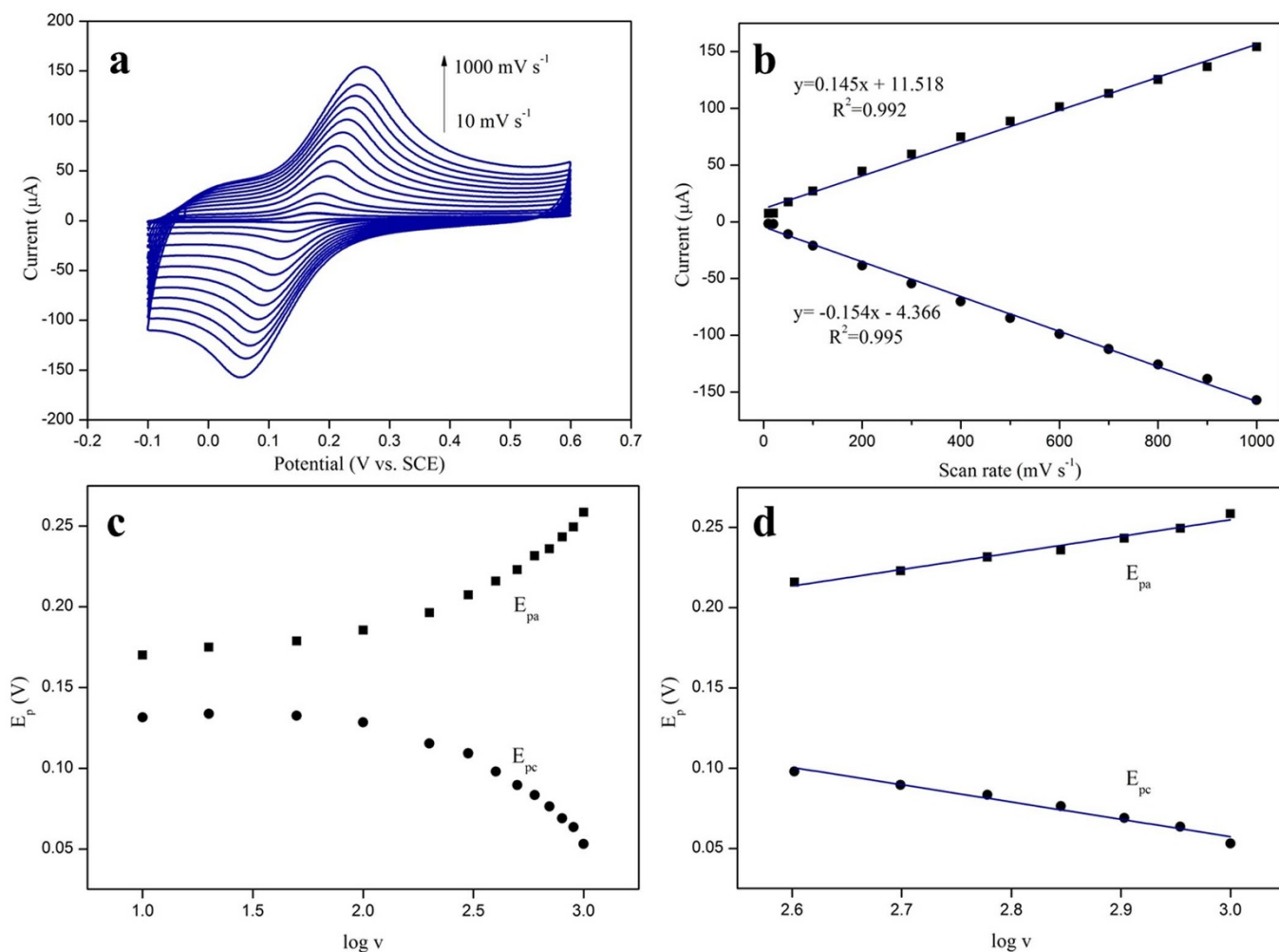

Figure 6 | (a) Cyclic voltammograms obtained for rGO/TiO$_2$ {001} modified GCEs in the presence of 0.5 mM DA in 0.1 M PBS (pH = 6.5) with various scan rates (10, 20, 50, 100, 200, 300, 400, 500, 600, 700, 800, 900 and 1000 mV s^{-1}). (b) Calibration plots of cathodic and anodic peak current *vs.* various scan rates. (c) Plot of variation in the E_p values *vs. log v*, with scan rates from 10–1000 mV s^{-1}. (d) Linear relationship between E_p values and *log v* with scan rates from 400–1000 mV s^{-1}.
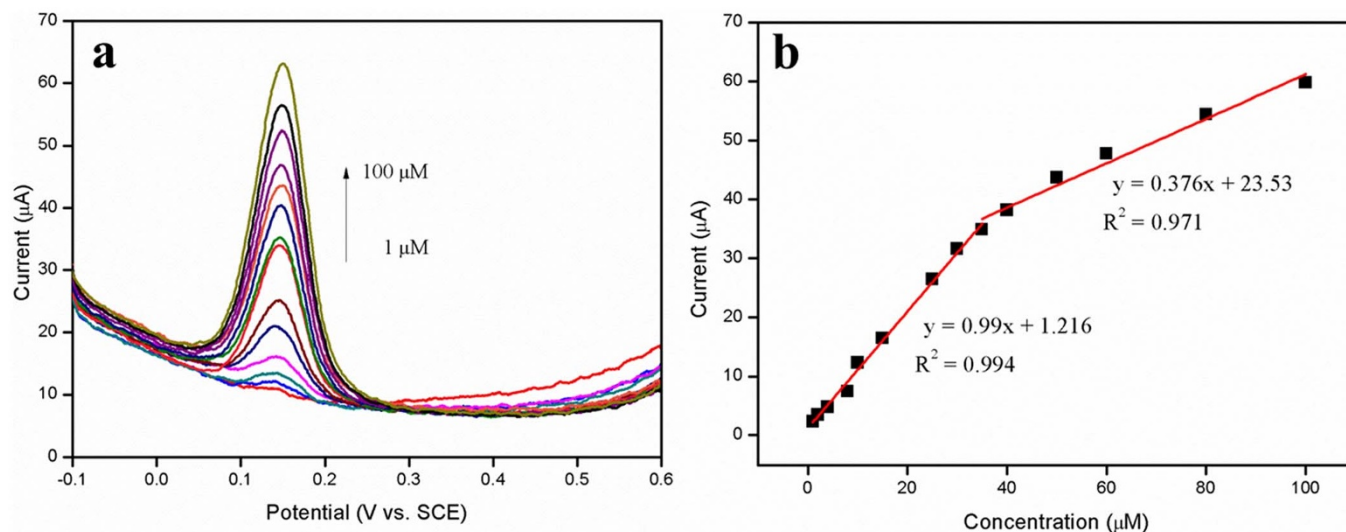
Figure 7 | (a) DPV obtained for rGO/TiO$_2$ {001} modified GCEs during the addition of 1, 2, 4, 8, 10, 15, 25, 30, 35, 40, 50, 60, 80, and 100 μM DA into the 0.1 M PBS (pH = 6.5). (b) Calibration plot observed for the oxidation peak current *vs.* concentration of DA.

and the scan rates (Figure 6b) clearly disclose that the electrochemical oxidation of DA at the rGO/TiO$_2$ {001} nanocomposite modified GCE is an adsorption controlled process[31]. In addition, E$_p$ values were plotted versus the logarithmic of the scan rate (Figure 6c) to obtain the kinetic parameters of electrochemical process. A linear relationship was only observed when the scan rate was above 400 mV s^{-1} (Figure 6d). According to Laviron theory, the linear slopes of E_{pa} and E_{pc} are $2.3RT/(1-\alpha)nF$ and $-2.3RT/\alpha nF$[32]. The calculated electron transfer coefficient, α was 0.55, which is consistent with the typical value of 0.5 observed for electrochemical reactions[33]. The charge transfer constant, k_s was evaluated using the following equation:

$$log\,k_s = \alpha log\,(1-\alpha) + (1-\alpha) log\,\alpha - log\,(RT/nFv)$$

$$\alpha(1-\alpha)nF\varDelta E_p/2.3RT$$

where, *v* is the scan rate; *n* is the number of transferred electrons; *F* is the Faraday constant and *R* and *T* are their usual significance. The k_s value was calculated as 2.748 ± 0.161 s^{-1}, which suggests that the electron transfer between the electrode and DA was improved by the addition of rGO/TiO$_2$ {001} nanocomposite on the surface of GCE.

Determination of DA at rGO/TiO$_2$ {001} modified GCE. To determine the detection limit (LOD) of DA in the presence of rGO/TiO$_2$ {001} modified GCE, the DPV technique was applied due to its increased current sensitivity. Figure 7a shows the anodic peak current observed at modified GCE with various concentrations of DA. It is noted that the anodic peak current increases with the addition of DA. Hence, by plotting a calibration graph (Figure 7b), two separate linear segments corresponding to different linear dynamic range (LDR) were observed. The first linear segment (y = 0.99x + 1.216) corresponds to LDR from 1–35 μM, while the second linear segment (y = 0.376x + 23.53) ranges from 35–100 μM. It was observed that the decrease in current sensitivity led to a lower response, resulting from the kinetic limitation of the rGO/TiO$_2$ {001} modified GCE[34]. Hence, based on the lower range, the LOD (S/N = 3) was estimated as 1.5 μM.

Simultaneous determination of DA and AA at rGO/TiO$_2$ {001} modified GCE. The overlapping voltammetric response of AA and DA causes problems towards their simultaneous detection, owing to their similar peak potentials (see Supplementary Fig. S5 online). This was clearly shown in Fig.S5a in the presence of bare GCE, where the peak potentials of AA and DA occur at same position resulting in

overlapped peaks. By modification of the GCE with the rGO/TiO$_2$ {001} nanocomposite, the DPV (in Fig. S5b) shows good separation potential between the AA and DA at about 0.2 V. Hence, the good selectivity of the modified GCE can be successfully achieved which can be attributed to the different charge properties of DA and AA (positively-charge DA, negatively-charged AA) occurring at the rGO/TiO$_2$ {001} surface. As the concentration of DA was increased in the presence of 1 mM AA, good selectivity was still exhibited by the modified GCE as there was no obvious change in the AA's peak current as a consequence of dismissing its tendency to interfere with DA (Figure 8a). In addition, a linear relationship between the concentration of DA and peak current was observed in two different linear segments (Figure 8b). The detection limit for the determination of DA in the presence of AA was calculated as 6 μM with LDR from 2–60 μM.

In the case of AA, a similar increasing trend was observed when the concentration of AA was increased in the presence of 100 μM DA (Figure 8c). However, the peak potentials of the electroactive species were seen shifted to the right when more AA was added. This is probably due to the acidic nature of AA as a weak acid that changes the pH of the PBS solution. It is understood that the pH of the solution affects the shifting of the analyte peak potentials[28]. Figure 8d reveals the calibration plot of current versus concentration of AA in the presence of 100 μM DA in two different linear segments. Therefore, the detection limit of AA was calculated as 200 μM with LDR 0.4–4 mM.

In summary, we have reported the first time, the preparation of TiO$_2$ with highly exposed {001} facets decorated with rGO sheets modified electrode based electrochemical sensor for the detection of dopamine (DA) in the presence of ascorbic acid (AA). A simple solvo-thermal method was employed to synthesize the rGO/TiO$_2$ nanocomposite with highly exposed {001} facets, which was used to modify glassy carbon electrode (GCE) for electrochemical sensing. The rGO/TiO$_2$ {001} modified GCE showed higher electrocatalytic activity towards the oxidation of DA over the other electrodes, such as bare GCE, TiO$_2$ {101}, TiO$_2$ {001}, rGO, rGO/TiO$_2$ {101} modified GCE. The rapid electron transfer and good electrocatalytic activity towards the oxidation of DA in the presence of AA was achieved by the rGO/TiO$_2$ {001} nanocomposite modified GCE. In addition, the modified GCE showed high sensitivity and good selectivity towards the detection of DA and AA. We anticipate that this initial study of the rGO/TiO$_2$ composite with highly exposed {001} facet features with further improvements could be potentially used for electrochemical sensing applications.

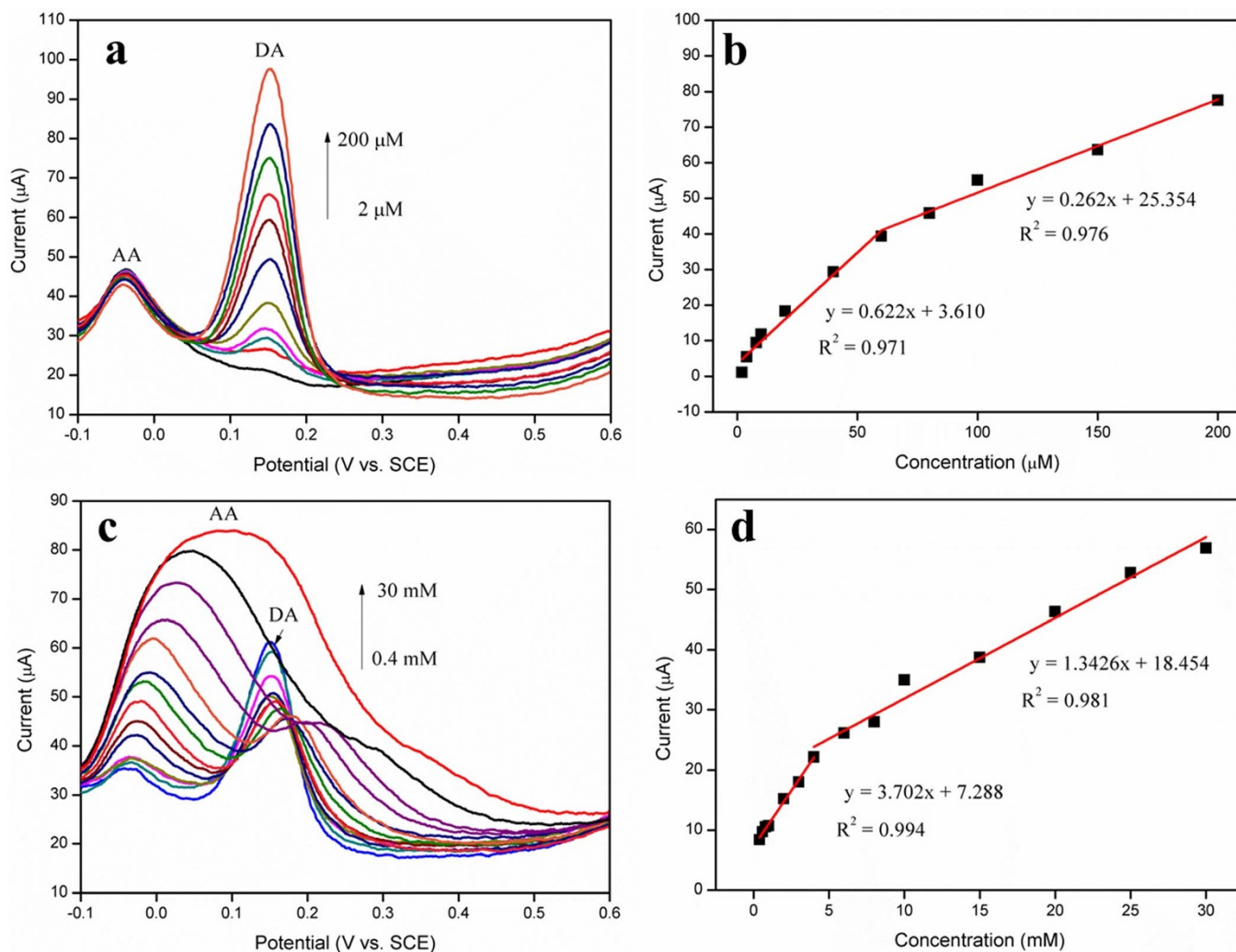**Figure 8** | (a) DPV obtained for rGO/TiO$_2$ {001} modified GCEs with 2, 4, 8, 10, 20, 40, 60, 80, 100, 150, and 200 μM DA in 0.1 M PBS (pH = 6.5) in the presence of 1 mM AA. (b) Calibration plot of oxidation peak current *vs.* concentration of DA containing 1 mM AA. (c) DPV obtained for rGO/TiO$_2$ {001} modified GCEs with 0.4, 0.6, 0.8, 1, 2, 3, 4, 6, 8, 10, 15, 20, 25, and 30 mM AA in 0.1 M PBS (pH = 6.5) containing 100 μM DA. (d) Calibration plot of oxidation peak current *vs.* concentration of AA containing 100 μM DA.

Experimental Details

Materials. Chemical reagents such as potassium permanganate (KMnO$_4$), tetraisopropylorthotitanate (TIPT), diethylenetriamine (DETA) and 3-hydroxytyraminium chloride (C$_8$H$_{12}$ClNO$_2$) were purchased from Merck, USA. Sulphuric acid (H$_2$SO$_4$), phosphoric acid (H$_3$PO$_4$), hydrochloric acid (HCl), hydrogen peroxide (H$_2$O$_2$), disodium hydrogen phosphate dehydrate, sodium dihydrogen phosphate, potassium chloride (KCl) and isopropyl alcohol were obtained from Systerm, Malaysia. Graphite flakes were received from Asbury Graphite Mills Inc. Potassium hexa-cyanoferrate(III) was supplied by Sigma-Aldrich. Unless otherwise specified, high pure de-ionized distilled water was used for the preparation of samples and stock solutions.

Preparation of rGO/TiO$_2$ {001} nanocomposite. The rGO/TiO$_2$ {001} nanocomposite was prepared according to the following procedure. Initially, graphene oxide (GO) was prepared *via* a simplified Hummer's method[35]. The obtained GO was subjected to freeze drying (Martin Christ, ALPHA 1–2/LD plus freeze dryer) for 24 h. Around 40 mg of GO was dispersed in 40 mL of isopropyl alcohol by gentle sonication. Then, a desired volume of TIPT and DETA were drop-wise added in sequence into the GO solution. The reaction mixture was transferred to a Teflon lined autoclave which

was subjected to hydrothermal treatment process at 200°C for 24 h. After the hydrothermal treatment, the autoclave was brought down to room temperature by natural cooling, washed with ethanol thrice and the gathered sample was dried in a hot air oven over night. Finally, the rGO/TiO$_2$ {001} nanocomposite was calcinated in a muffle furnace at 400°C for 2 h at a heating rate of 1°C/min.

Characterization techniques. The morphological studies of synthesized rGO/TiO$_2$ {001} nanocomposite were carried out by using JEOL JSM-7600F field emission scanning electron microscope (FESEM) and JEOL JEM-2100F high resolution transmission electron microscope (HRTEM). The X-ray photoelectron spectroscopy (XPS) measurements were performed using synchrotron radiation from beamline no. 3.2 at Synchrotron Light Research Institute, Thailand. The Raman spectral data were obtained using Renishaw inVia Raman microscope system with a 514 nm laser beam.

Electrochemical studies. The rGO/TiO$_2$ {001} modified GC electrode was fabricated by dispersing 1 mg of the prepared rGO/TiO$_2$ {001} nanocomposite into 1 mL of high pure de-ionized double distilled water and then sonicated for 5 min to ensure homogeneous dispersion. Around 5 μL of nanocomposite suspension was drop casted on the polished GCE surface which was air dried at room

temperature and then placed on a hot air oven at 60°C for 30 min to obtain a stable rGO/TiO$_2$ {001} modified GCE. For comparison studies, the TiO$_2$ {101}, TiO$_2$ {001}, rGO, rGO/TiO$_2$ {101} modified GCE were fabricated by following the similar method. All the electrochemical measurements were carried out using VersaSTAT 3 electrochemical analyzer (Princeton Applied Research, USA) with a conventional three electrode system under nitrogen atmosphere at room temperature. The working electrode was nanocomposite modified GCE, platinum wire was used as a counter electrode and Na$_2$SO$_4$ saturated calomel electrode (SCE) was used as a reference electrode. A 0.1 M phosphate buffer solution ($pH = 6.5$) was used as a supporting electrolyte. All the potentials were quoted against SCE unless otherwise mentioned.

1. Sun, W. et al. Application of graphene–SnO$_2$ nanocomposite modified electrode for the sensitive electrochemical detection of dopamine. Electrochim. Acta 87, 317–322 (2013).
2. Li, J., Zhao, J. & Wei, X. A sensitive and selective sensor for dopamine determination based on a molecularly imprinted electropolymer of o-aminophenol. Sens. Actuators, B 140, 663–669 (2009).
3. Mo, J. W. & Ogorevc, B. Simultaneous measurement of dopamine and ascorbate at their physiological levels using voltammetric microprobe based on overoxidized poly(1,2-phenylenediamine)-coated carbon fiber. Anal. Chem. 73, 1196–1202 (2001).
4. Yang, L., Liu, D., Huang, J. & You, T. Simultaneous determination of dopamine, ascorbic acid and uric acid at electrochemically reduced graphene oxide modified electrode. Sens. Actuators, B 193, 166–172 (2014).
5. Cai, W., Lai, T., Du, H. & Ye, J. Electrochemical determination of ascorbic acid, dopamine and uric acid based on an exfoliated graphite paper electrode: A high performance flexible sensor. Sens. Actuators, B 193, 492–500 (2014).
6. Fan, Y. et al. Hydrothermal preparation and electrochemical sensing properties of TiO$_2$-graphene nanocomposite. Colloids Surf., B 83, 78–82 (2011).
7. Xu, C.-X. et al. Simultaneous electrochemical determination of dopamine and tryptophan using a TiO$_2$-graphene/poly(4-aminobenzenesulfonic acid) composite film based platform. Mater. Sci. Eng., C 32, 969–974 (2012).
8. Pan, J. H., Han, G., Zhou, R. & Zhao, X. S. Hierarchical N-doped TiO$_2$ hollow microspheres consisting of nanothorns with exposed anatase {101} facets. Chem. Commun. 47, 6942–6944 (2011).
9. Chen, J. S. et al. Constructing hierarchical spheres from large ultrathin anatase TiO$_2$ nanosheets with nearly 100% exposed (001) facets for fast reversible lithium storage. J. Am. Chem. Soc. 132, 6124–6130 (2010).
10. Liuan, G. et al. One-step preparation of graphene supported anatase TiO$_2$ with exposed {001} facets and mechanism of enhanced photocatalytic property. ACS Appl. Mater. Interfaces 5, 3085–93 (2013).
11. Sun, C. H. et al. Higher charge/discharge rates of lithium-ions across engineered TiO$_2$ surfaces leads to enhanced battery performance. Chem Commun. 46, 6129–6131 (2010).
12. Wang, H., Liu, M., Yan, C. & Bell, J. Reduced electron recombination of dye-sensitized solar cells based on TiO$_2$ spheres consisting of ultrathin nanosheets with [001] facet exposed. Beilstein J. Nanotechnol. 3, 378–387 (2012).
13. Wang, W., Lu, C., Ni, Y. & Xu, Z. Crystal facet growth behavior and thermal stability of {001} faceted anatase TiO$_2$: mechanistic role of gaseous HF and visible-light photocatalytic activity. CrystEngComm 15, 2537–2543 (2013).
14. Zhu, L., Liu, K., Li, H., Sun, Y. & Qiu, M. Solvothermal synthesis of mesoporous TiO$_2$ microspheres and their excellent photocatalytic performance under simulated sunlight irradiation. Solid State Sci. 20, 8–14 (2013).
15. Naumenko, D., Snitka, V., Snopok, B., Arpiainen, S. & Lipsanen, H. Graphene-enhanced Raman imaging of TiO$_2$ nanoparticles. Nanotechnology 23, 465703 (2012).
16. Zheng, Q. et al. Highly transparent and conducting ultralarge graphene oxide/single-walled carbon nanotube hybrid films produced by Langmuir–Blodgett assembly. J. Mater. Chem 22, 25072 (2012).
17. Thakur, S. & Karak, N. Green reduction of graphene oxide by aqueous phytoextracts. Carbon 50, 5331–5339 (2012).
18. Eigler, S., Dotzer, C. & Hirsch, A. Visualization of defect densities in reduced graphene oxide. Carbon 50, 3666–3673 (2012).
19. Zhang, H. et al. A facile one-step synthesis of TiO$_2$/graphene composites for photodegradation of methyl orange. Nano Res. 4, 274–283 (2010).
20. Gao, Y., Ma, D., Wang, C., Guan, J. & Bao, X. Reduced graphene oxide as a catalyst for hydrogenation of nitrobenzene at room temperature. Chem. Commun. 47, 2432–2434 (2011).
21. Dreyer, D. R., Park, S., Bielawski, C. W. & Ruoff, R. S. The chemistry of graphene oxide. Chem. Soc. Rev. 39, 228–240 (2010).
22. Pei, S., Zhao, J., Du, J., Ren, W. & Cheng, H.-M. Direct reduction of graphene oxide films into highly conductive and flexible graphene films by hydrohalic acids. Carbon 48, 4466–4474 (2010).
23. Allam, N. K., Alamgir, F. & El-sayed, M. A. Enhanced photoassisted water electrolysis using vertically oriented anodically fabricated Ti−Nb−Zr−O mixed oxide nanotube arrays. ACS Nano 4, 5819–5826 (2010).
24. Dong, F., Guo, S., Wang, H., Li, X. & Wu, Z. Enhancement of the visible light photocatalytic activity of C-doped TiO$_2$ nanomaterials prepared by a green synthetic approach. J. Phys. Chem. C 115, 13285–13292 (2011).
25. Zhuang, Z., Li, J., Xu, R. & Xiao, D. Electrochemical Detection of Dopamine in the Presence of Ascorbic Acid Using Overoxidized Polypyrrole/Graphene Modified Electrodes. Int. J. Electrochem. Sci. 6, 2149–2161 (2011).
26. Zhang, Q. et al. Mn$_3$O$_4$/graphene composite as counter electrode in dye-sensitized solar cells. RSC Adv. 4, 15091 (2014).
27. Gao, M., Peh, C. K. N., Ong, W. L. & Ho, G. W. Green chemistry synthesis of a nanocomposite graphene hydrogel with three-dimensional nano-mesopores for photocatalytic H$_2$ production. RSC Adv. 3, 13169 (2013).
28. Mahshid, S. S. S. et al. Sensitive determination of dopamine in the presence of uric acid and ascorbic acid using TiO2 nanotubes modified with Pd, Pt and Au nanoparticles. Analyst 136, 2322–2329 (2011).
29. Naik, R. R. et al. Separation of ascorbic acid, dopamine and uric acid by acetone/water modified carbon paste electrode: A cyclic voltammetric study. Int. J. Electrochem. Sci. 4, 855–862 (2009).
30. Huang, D., Chen, C., Wu, Y., Zhang, H. & Sheng, L. The determination of dopamine using glassy carbon electrode pretreated by a simple electrochemical method. Int. J. Electrochem. Sci. 7, 5510–5520 (2012).
31. Yang, A. et al. A simple one-pot synthesis of graphene nanosheet/SnO$_2$ nanoparticle hybrid nanocomposites and their application for selective and sensitive electrochemical detection of dopamine. J. Mater. Chem. B 1, 1804 (2013).
32. Laviron, E. General expression of the linear potential sweep voltammogram in the case of diffusionless electrochemical systems. J. Electroanal. Chem. 101, 19–28 (1979).
33. Skulason, E. et al. Density functional theory calculations for the hydrogen evolution reaction in an electrochemical double layer on the Pt(111) electrode. Phys. Chem. Chem. Phys. 9, 3241–3250 (2007).
34. Mazloum-ardakani, M., Rajabi, H., Beitollahi, H., Bi, B. & Mirjalili, F. Voltammetric determination of dopamine at the surface of TiO$_2$ nanoparticles modified carbon paste electrode. Int. J. Electrochem. Sci. 5, 147–157 (2010).
35. Marcano, D. C. et al. Improved synthesis of graphene oxide. ACS Nano 4, 4806–4814 (2010).

Acknowledgments

Author contributions

G.T.S.H. wrote the main manuscript text and prepared all figures in text. A.P., H.N.M. and L.H.N. reviewed the manuscript content.

Additional information